Novel Modulation of Isolated Bidirectional DC–DC Converter for Energy Storage Systems

Nguyen Anh Dung, *Student Member, IEEE*, Huang-Jen Chiu, *Senior Member, IEEE*, Jing-Yuan Lin, *Member, IEEE*, Yao-Ching Hsieh, *Member, IEEE*, Hui-Ting Chen, and Bo-Xiang Zeng

***Abstract*—In this study, a novel modulation of an isolated three-phase bidirectional dc–dc converter is proposed for the high-voltage input power supply to low-voltage output energy storage systems. The wye-delta connection of the transformers is employed to reduce the voltage stress at the high side and the current stress at the low side of the transformers. Frequency control allows the output voltage regulation, and a phase-shift algorithm with a resonant tank is proposed following with the switching frequency to reduce the frequency range with the specific power. Furthermore, the zero-voltage-switching condition for all MOSFETs in the entire power range, which is the major restriction of a single-phase converter, is also discussed in this paper. The three-phase wye-delta converter significantly reduces the ripple of inductor current compared with that of a single-phase converter. A 2 kW prototype converter was built and successfully tested to verify the capability of such control modulation.**

***Index Terms*—Bidirectional converter, frequency modulation, phase-shift algorithm, three-phase wye-delta converter.**

I. Introduction

RENEWABLE energy resources have been paid significant attention due to the limitation of oil resource and their pollution. However, such energy resources are unstable and easily lead to an intermittent trouble, so it is difficult to supply directly to the output without any protection or backup. Therefore, the energy storage systems (ESSs) have been proposed and widely used in so many applications [1]. These storage systems, such as batteries or ultracapacitors, store the energy during the over-supplying power and play as a power source during the disruption of renewable energy resources. A bidirectional converter is the best candidate to transfer these energy resources to the ESSs and supply the energy from ESSs to the load because of its bidirectional flows, reliability, and easy control. Two

Manuscript received October 11, 2017; revised January 1, 2018 and February 22, 2018; accepted April 9, 2018. Date of publication April 16, 2018; date of current version December 7, 2018. This work was support by the Ministry of Science and Technology, Taiwan, under Grant MOST 106-2221-E-011-091-MY3. Recommended for publication by Associate Editor M. Amirabadi. *(Corresponding author: Huang-Jen Chiu.)*

N. A. Dung, H.-J. Chiu, J.-Y. Lin, H.-T. Chen, and B.-X. Zeng are with the Department of Electronics and Computer Engineering, National Taiwan University of Science and Technology, Taipei 10607, Taiwan (e-mail:

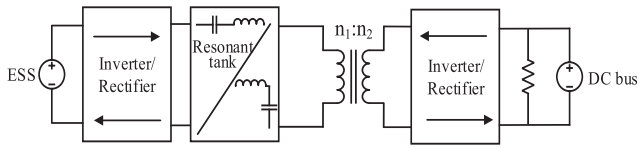

Fig. 1. Bidirectional resonant converters.

common topologies of the bidirectional dc–dc converters, namely, isolated and nonisolated converters exist. The nonisolated converters, such as buck–boost, Cuk, and single-ended primary inductance converter (SEPIC) converters, have been employed in some applications [2]–[5]. They possess advantages, such as simple circuitry, small size, low cost, and the simple controller. However, no protection exists between the batteries and dc-bus because of the nonisolation, and the reliability and safety of the dc-bus and batteries need to be concerned. Moreover, the zero-voltage-switching (ZVS) condition of all switches needs to be considered carefully; in other words, it is very hard to design the topology and controller to achieve the ZVS in the whole power range, results in low efficiency especially at light-load condition. Voltage gain is also one of their limitations. The multilevel converter can fulfill the voltage gain but the complicated configuration is a drawback. Therefore, isolated converters are employed to adjust the output voltage for specific applications with the simple circuit [6]–[25]. The output can be regulated at low or high voltage depending on the transformer turn ratio without affecting the voltage gain. Flyback and forward converters are constructed to some small and medium power applications [6]. However, the required components are a trouble for specific applications because of the high stress on the switches. Dual active bridge converter has been employed in high-power applications [7]–[13]. Nevertheless, the ZVS range is very narrow. Therefore, the efficiency is poor, especially at light-load condition. Single-phase-shift control, dual-phase-shift control, and triple-phase-shift control are used. However, these controllers cannot cover the ZVS for all power range and are becoming increasingly complicated. Many operation modes occur in the entire power range, and the transition is a significant problem. Converters with a resonant tank are employed to extend the ZVS range [14], [15]. Fig. 1 shows the schematic of general resonant converters. Some topologies, such as series resonant, parallel resonant, and their combination, are utilized. The series resonant converter (SRC) was proposed to apply in the step-down system. However, SRCs produce high

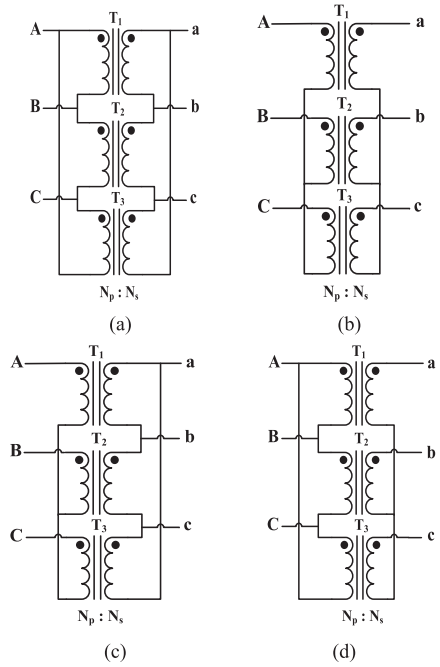

Fig. 2. Three-phase connection. (a) Delta-delta. (b) Wye-wye. (c) Wye-delta. (d) Delta-wye.

inductor current ripple and result in high rms current, and the conduction loss is high even in the light-load condition. The switching frequency range leads to the difficulty of the resonant tank design to fulfill the ZVS in the entire power range. The three-phase converter can reduce the inductor current ripple by sharing the energy [16]–[25]. The three-phase transformer connection possesses four combinations: wye-wye, wye-delta, delta-wye, and delta-delta. The connection of the four combinations is shown in Fig. 2. The wye connection is usually used in high-voltage applications. The voltage stress on the transformer of wye connection is always lower than the input because of its characteristic. The delta connection is employed in high-current applications because of its lower current stress on transformer and reliability compared with those of the wye connection. The three-phase isolated dc–dc resonant converter has been studied in some applications [26]. However, the design considerations such as voltage and current stress of the transformer, ZVS condition in the whole power range have not been analyzed and verified carefully. In [19], the ZVS condition for MOSFETs was analyzed in detail. However, the ZVS range is narrow due to the limitation of the control method. Since almost studies aimed to propose the unidirectional flows, they cannot be used for the ESS in which bidirectional flows are required [27], [28]. Moreover, since the diodes or the synchronous switches are employed in the secondary side, there is the fixed phase shift between the primary and secondary sides [26], [27]; in other words, the frequency control scheme was proposed for these topologies. Therefore, the frequency range needs to be considered in the wide power range applications.

This study proposes the three-phase bidirectional converter and its novel control scheme. This topology can fulfill the drawbacks of single-phase converters and SRCs. The low side of this topology is an ESS with low voltage rating and high power, and it requires the delta connection to overcome the problem of reliability and to reduce the current stress of the transformer. The high side of this circuit is a dc-bus or renewable energy resources with high voltage rating. Wye connection is employed to reduce the voltage stress of the transformer. The ZVS condition for the entire power range of all MOSFETs is also discussed. Moreover, the phase shift control algorithm allows the reduction of the switching frequency range significantly. A 2 kW prototype was successfully built and tested to verify the contribution of this work.

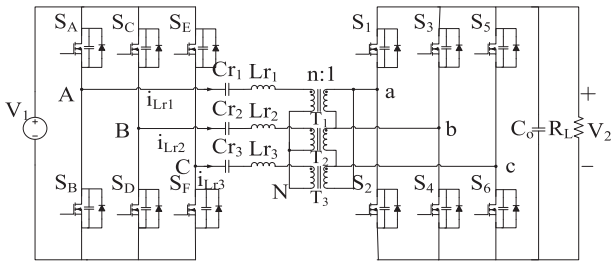

Fig. 3. Three-phase bidirectional wye-delta converter.

II. Novel Control Modulation of a Bidirectional Wye-Delta Converter

The circuit schematic of the three-phase bidirectional wye-delta converter is shown in Fig. 3. Switches S_A–S_F and S_1–S_6 are controlled at 0.5 duty ratio. The system transfers the energy from the primary side dc-bus V_1 to the secondary side battery V_2 in the buck mode. In the opposite-side power flow direction, the battery V_2 plays as a power source to transfer the energy to the dc-bus V_1 in boost mode. The turn ratio between the primary and the secondary side of the transformer is defined as n. Three legs in the primary side and three legs in the secondary side exhibit phase shifts at 120° and 240°, respectively. Phase shift ϕ between the primary and secondary sides is proposed to control the power flows and reduce the switching frequency range of the circuit. In other words, switches S_A and S_1 possess phase shift ϕ, switches S_C and S_3 obtain phase shift $(120^\circ + \phi)$ and switches S_E and S_5 possess phase shift $(240^\circ + \phi)$. The lower leg switch is symmetrical with the upper switch in the same leg. The switching frequency f_s of the system is also controlled to regulate the output voltage.

The basic idea about the SRC has been discussed in many papers [25]–[27]. In this study, a series resonant tank is employed to achieve the ZVS of MOSFETs. The equivalent circuit of phase one is depicted in Fig. 4, and phases two and three possess the same equivalent circuit. The resonant frequency f_r and impedance Z depend on the resonant inductor L_{r1}, resonant capacitor C_{r1}, and are expressed as

$$f_r = \frac{1}{2\pi\sqrt{Lr_1 Cr_1}} \tag{1}$$

$$Z = j2\pi f_s Lr_1 + \frac{1}{j2\pi f_s Cr_1}. \tag{2}$$

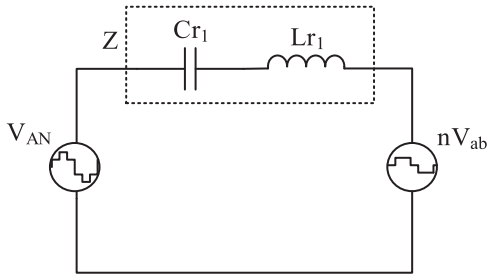

Fig. 4. Equivalent circuit of phase one.

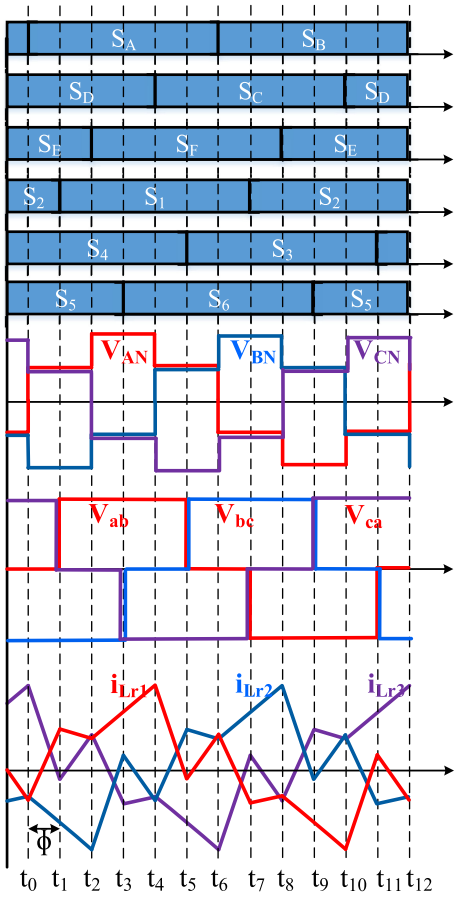

Fig. 5. Timing diagram of the proposed control modulation.

The impedance Z is the same at every phase in the three-phase converter. As the feature of the SRC, switching frequency f_s is higher than the resonant frequency to fulfill the ZVS for MOSFETs. The timing diagram in accordance with this basic operation is proposed in Fig. 5. The phase shift ϕ between switches S_A and S_1 is controllable. This phase shift can be calculated by the power transfer. The equivalent circuits of all intervals are shown in Fig. 6(a)–(f). The primary transformer voltage is operated in six steps, and the secondary transformer voltage is controlled in three steps. The zero state of the secondary transformer voltage is created by the wye-delta connection. This zero state can reduce the converter circulating current and results in a low power loss in the transformer. The timing diagram presents that the inductor current is symmetrical in one switching period. Therefore, only the positive part of the inductor current is analyzed and the negative part is omitted. We assume that the components are the same in three phases and the inductor current of three phases can be expressed as

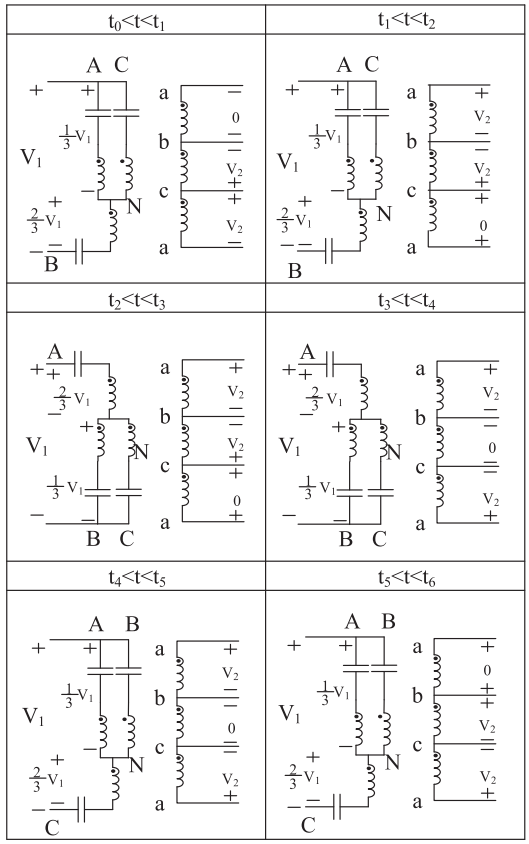

Fig. 6. Equivalent circuit of the three-phase converter.

$$\begin{cases} I_{Lr1} = \dfrac{V_{AN} - nV_{ab}}{Z} \\ I_{Lr2} = \dfrac{V_{BN} - nV_{bc}}{Z} \\ I_{Lr3} = \dfrac{V_{CN} - nV_{ca}}{Z} \end{cases} \tag{3}$$

$$V_{AN} = \begin{cases} \dfrac{1}{3}V_1, & (t_0 \le t < t_2) \\ \dfrac{2}{3}V_1, & (t_2 \le t < t_4) \\ \dfrac{1}{3}V_1, & (t_4 \le t < t_6) \end{cases} \tag{4}$$

$$V_{ab} = \begin{cases} 0, & (t_0 \le t < t_1) \\ V_2, & (t_1 \le t < t_5) \\ 0, & (t_5 \le t < t_6). \end{cases} \tag{5}$$

Assumed that one switching period can be transformed to (2π) without the approximation. Fig. 7 shows the timing diagram of phase one in one switching cycle. It can be seen that the inductor current $I_{Lr1} = I_{Lr2} = I_{Lr3}$ with the phase shift of 120° and 240°, respectively; therefore, only phase one is

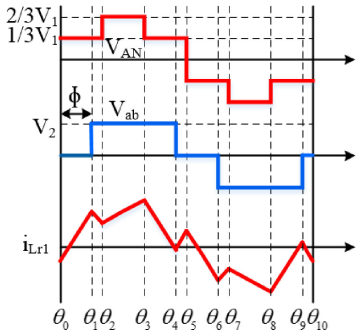

Fig. 7. Equivalent diagram of the inductor current of phase one.

analyzed for simplified calculation. The operating principle indicates that voltage ratio $M_G = nV_2/V_1$ can be used to simplify the calculation of the inductor current. The timing diagram also implies that

$$i_{Lr1}(\theta_0) = -i_{Lr1}(\pi) = -\frac{2\pi V_{AN} - 3\pi M_G V_{AN}}{9|Z|} \tag{6}$$

$$\begin{cases} i_{Lr1}(\theta) = \dfrac{V_{AN}(3\theta - 2\pi + 3\pi M_G)}{9|Z|}, \\ \qquad\qquad (\theta_0 \le \theta < \theta_1) \\ i_{Lr1}(\theta) = \dfrac{V_{AN}(3\theta - 2\pi + 3\pi M_G - 9\theta M_G + 9\phi M_G)}{9|Z|}, \\ \qquad\qquad (\theta_1 \le \theta < \theta_2) \\ i_{Lr1}(\theta) = \dfrac{V_{AN}(2\theta - \pi + \pi M_G - 3\theta M_G + 3\phi M_G)}{3|Z|}, \\ \qquad\qquad (\theta_2 \le \theta < \theta_3) \\ i_{Lr1}(\theta) = \dfrac{V_{AN}(3\theta - \pi + 3\pi M_G - 9\theta M_G + 9\phi M_G)}{9|Z|}, \\ \qquad\qquad (\theta_3 \le \theta < \theta_4) \\ i_{Lr1}(\theta) = -\dfrac{V_{AN}(\pi - 3\theta + 3\pi M_G)}{9|Z|}, \\ \qquad\qquad (\theta_4 \le \theta < \theta_5) \end{cases} \tag{7}$$

where

$$\begin{cases} \theta_0 = 0 \\ \theta_1 = \phi \\ \theta_2 = \pi/3 \\ \theta_3 = 2\pi/3 \\ \theta_4 = 2\pi/3 + \phi \\ \theta_5 = \pi. \end{cases}$$

Then, the power transfer can be calculated by the energy from the primary side send to the secondary side

$$P_{\mathrm{tr},1\phi} = \int_0^{\pi} V_{AN}(\theta) i_{Lr1}(\theta) d\theta = \frac{M_G V_1^2 (6\phi - \pi)}{18|Z|}. \tag{8}$$

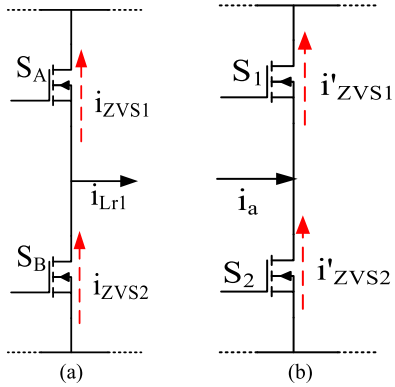

Fig. 8. Inductor current direction. (a) Primary side. (b) Secondary side.

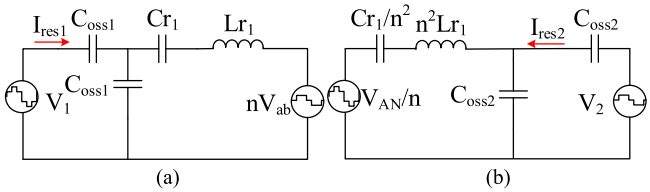

Fig. 9. Equivalent circuit. (a) Before MOSFET SA turns ON. (b) Before MOSFET S_1 turns ON.

The power transfer of the three-phase bidirectional wye-delta converter can be expressed as

$$P_{\mathrm{tr},3\phi} = 3P_{\mathrm{tr},1\phi} = \frac{M_G V_1^2 (6\phi - \pi)}{6|Z|}. \tag{9}$$

The output power can be estimated by the efficiency η as follows:

$$P_{\mathrm{out}} = \eta P_{\mathrm{tr},3\phi} = \frac{\eta M_G V_1^2 (6\phi - \pi)}{6|Z|}. \tag{10}$$

III. ZVS Condition

The inductor currents of the primary and secondary sides of phase one are shown in Fig. 8(a) and (b), respectively. The body diode of the upper MOSFET of the primary side should be conducted prior to the switch turn ON. The current should be at the direction of i_{ZVS1} direction, as shown in Fig. 8(a). In other words, the inductor current i_{Lr1} is negative, and its absolute value should be higher than that of the resonant current I_{res1} formed by the resonant tank and the output parasitic capacitance of the MOSFETs. Fig. 9(a) shows the equivalent circuit of this resonance before MOSFET S_A turns ON. Similarly, the inductor current should be positive to achieve ZVS for the lower MOSFET. When current $i_{Lr1}(\theta_0)$ is negative, the ZVS condition for switch S_B is also fulfilled because of the symmetry of the inductor current, as shown in Fig. 5. The ZVS condition of switches S_A

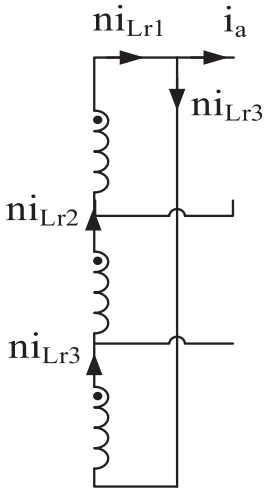

Fig. 10. Feature of inductor current at the secondary side.

can be expressed as

$$i_{Lr1}(\theta_0) = -\frac{2\pi V_1 - 3\pi M_G V_1}{27|Z|} \le -I_{\text{res1}} \tag{11}$$

$$\Rightarrow M_G \le \frac{2 - \frac{27|Z|I_{\text{res1}}}{\pi V_1}}{3} \tag{12}$$

$$I_{\text{res1}} = V_1\sqrt{\frac{2C_{\text{oss1}}Cr}{(2C_{\text{oss1}}+Cr)Lr}}. \tag{13}$$

At MOSFET S_1 of the secondary side, the body diode should be conducted before S_1 turns ON, or inductor current i_a is positive and higher than the resonant current formed by the effect of the primary resonant tank and the parasitic capacitance of the secondary side MOSFET, as shown in Fig. 9(b). For MOSFET S_2, inductor current i_a is negative to achieve ZVS. Switch S_2 achieves ZVS requirement because of the symmetry of the inductor current. As shown in Fig. 10, the inductor current of phase one in the secondary side can be calculated as

$$i_a = n(i_{Lr1} - i_{Lr3}). \tag{14}$$

To achieve ZVS for switch S_1, the inductor i_a should be

$$i_a = n(i_{Lr1}(\theta_1) - i_{Lr3}(\theta_4)) \ge I_{\text{res2}} \tag{15}$$

where

$$I_{\text{res2}} = V_2\sqrt{\frac{2C_{\text{oss2}}Cr}{(2C_{\text{oss2}}+n^2Cr)Lr}} \tag{16}$$

$$\Rightarrow n\left[\frac{V_1(3\phi - 2\pi + 3\pi M_G)}{27|Z|} - \frac{-V_1(-3\phi - \pi + 3\pi M_G)}{27|Z|}\right] \ge I_{\text{res2}} \tag{17}$$

$$\Rightarrow M_G \ge \frac{\frac{9|Z|I_{\text{res2}}}{n\pi V_1} + 1}{2}. \tag{18}$$

The optimized voltage ratio M_G for the ZVS of all MOSFETs can be calculated by the minimum power transfer with

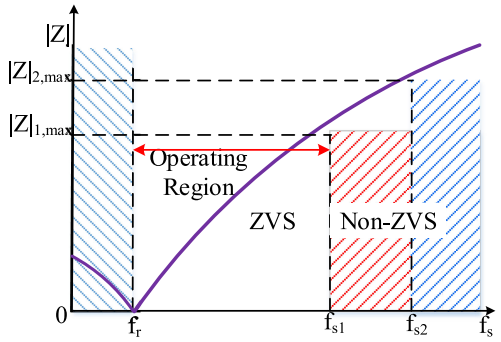

Fig. 11. ZVS condition of the three-phase bidirectional DC–DC converter.

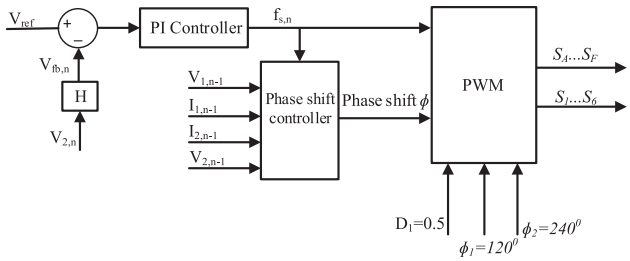

Fig. 12. Total loop controller of the bidirectional three-phase wye-delta converter.

maximum switching frequency, that is

$$\frac{\frac{9|Z|_{\max}I_{\text{res2}}}{n\pi V_1} + 1}{2} \le M_G \le \frac{2 - \frac{27|Z|_{\max}I_{\text{res1}}}{\pi V_1}}{3}. \tag{19}$$

From the specification, the voltage ratio M_G is chosen with the condition from (19). From (12) and (18), the condition of the impedance Z can be calculated by

$$\begin{cases} |Z|_{1,\max} \le \dfrac{\pi V_1(2-3M_G)}{27I_{\text{res1}}} \\ |Z|_{2,\max} \le \dfrac{n\pi V_1(2M_G-1)}{9I_{\text{res2}}}. \end{cases} \tag{20}$$

The switching frequency range for ZVS condition is calculated by (20) with the value of the resonant tank and shown in Fig. 11. Whenever the circuit operates within the ZVS condition, the ZVS can be achieved for all MOSFETs. In the conventional SRC, the ZVS condition is limited by the maximum switching frequency. The range of switching frequency is wide, and the ZVS range is wider. However, the design of the resonant tank and the electromagnetic interference noise are problems with the wide switching frequency. In this novel control design, the switching frequency range is highly dependent on the voltage gain M_G, as shown in (20). Moreover, the phase shift control scheme is employed to reduce the range of switching frequency. As shown in (10), power is controlled not only by the switching frequency but also by the variable phase shift. Therefore, the frequency range can be limited to a small range, and the phase shift can be calculated in parallel with the frequency to optimize the power transfer with the best "switching frequency point." The control modulation of the bidirectional three-phase wye-delta converter is shown in Fig. 12. Two blocks exist: the first block is a proportional-integral (PI) controller, which is used

TABLE I
COMPARISON OF THE SINGLE-PHASE RESONANT CONVERTER, WYE-WYE RESONANT CONVERTER, AND THE PROPOSED CONVERTER

Parameters	Single-phase resonant converter	Wye-wye resonant converter	Proposed converter
Control modulation	Frequency or phase shift	Frequency	Frequency and phase shift
Primary transformer voltage stress	V_1	$\frac{2V_1}{3}$	$\frac{2V_1}{3}$
ZVS range	Narrow	Medium	Very wide
Frequency range	Wide	Medium	Narrow
Operation region	LLC in forward, SRC in reverse and vice versa	LLC in forward, SRC in reverse and vice versa	SRC in both forward and reverse flows

TABLE II
KEY PARAMETERS OF THE BIDIRECTIONAL THREE-PHASE WYE-DELTA CONVERTER

Parameter			Value
Input voltage		V_1	390–420 Vdc
Output voltage		V_2	48 Vdc
Maximum power		P_{max}	2 kW
Switching frequency		f_s	101–150 kHz
Resonant frequency		f_r	100 kHz
Phase shift range		ϕ	$\pi/12-\pi/4$
Magnetics	Inductor	L	12 µH
		R_s	40 mΩ
		Turns	10
	Transformer	L_{lk}	8 µH
		L_m	300 µH
		Turn ratio	14:3
		$R_{s,p}$	40 mΩ
		$R_{s,s}$	16 mΩ
Primary switch	IPI60R099CP	$R_{DS,\,ON}$	0.099 Ω
		C_{OSS1}	130 pF
Secondary switch	IXFN230N20T	$R_{DS,ON}$	7.5m Ω
		C_{OSS2}	2440 pF
Controller	TMS320F28035		

to regulate the output voltage by frequency control. The second block is the phase-shift control algorithm. This block receives the voltage and current. The phase shift can be calculated based on (10) with the estimation of the previous efficiency. There will be a small error between the calculation and the real model because the present efficiency is unknown. However, this error is small and can be neglected because the previous efficiency $\eta(n-1)$ can be determined. From (10), the initial value of the phase shift is 30°. The duty ratio $D_1 = 0.5$ is employed for all MOSFETs. Moreover, phase shifts ϕ_1 and ϕ_2 are the phase shifts between phase two and phase three to phase one in the primary and secondary sides, respectively. In the pulsewidth modulation block, the evaluation of switching frequency and double checking with (11) and (15) are employed to ensure that all MOSFETs achieve ZVS. The transition between previous switching frequency $f_s(n-1)$ and current switching frequency $f_s(n)$ is checked to ensure that no significant step occurs from $f_s(n-1)$ to $f_s(n)$ because the frequency control with phase shift is sensitive to output change. The comparison of the proposed modulation with the single-phase resonant converter and the bidirectional three-phase wye-wye converter is discussed in Table I. In the single-phase resonant converter, the frequency modulation is popularly employed to regulate the output. However, the power range is smaller than the three-phase resonant converter. Moreover, the ZVS is limited by the switching frequency; or, the ZVS range is narrow compared with the three-phase resonant converter at the same power rating because of the limitation of the resonant tank design. Furthermore, the voltage and current stress of the transformer is higher since only single-phase converter covers all the load. The three-phase wye-wye converter can reduce the stress on every switch. However, the ZVS is also limited because the wye-wye connection can be considered as three single-phase converters. Moreover, the control modulation limits the ZVS because of the limitation of the switching frequency range. The range of the switching frequency is wider, the design of the resonant tank is harder. Additionally, the design of the resonant tank to operate the system in forward and reverse mode is a big issue since the forward mode can be operated in inductor-inductor-capacitor (LLC) region and reverse mode is modulated in SRC region and vice versa. Therefore, the switching frequency range should be considered very carefully. The proposed modulation is only operated in the SRC mode for both forward and reverse modes. The phase shift is employed to control the direction of the power flow and to reduce the burden of the switching frequency. Therefore, the frequency range is smaller within the ZVS range in the whole power range.

IV. SIMULATION AND EXPERIMENTAL VERIFICATIONS

A 2 kW prototype with the resistor load was built and successfully tested to verify the feasibility of the control modulation. The specification of this topology is shown in Table II. Assumed that at maximum phase shift, the maximum power transfer can be calculated by the maximum impedance *Z* as shown in (20). In other words, the power transfer can be higher at the smaller impedance *Z*; or, the range of the power transfer could be higher than the original design. Therefore, the limitation of the impedance *Z* can be expressed as

$$P_{\mathrm{tr},3\phi,\max} = \frac{M_G V_1^2 (6\phi_{\max} - \pi)}{6|Z|_{\max}} \tag{21}$$

where $\phi_{\max} = \pi/4$ and $P_{\mathrm{tr},3\phi,\max}$ is the maximum power of the prototype, the maximum impedance can be calculated from the voltage ratio M_G. From (12), (13), and (21), the resonant capacitance and inductance can be calculated as

$$\begin{cases} f_r = \dfrac{1}{2\pi\sqrt{L_r C_r}} \\ M_G \le \dfrac{2 - \dfrac{27|Z|_{\max} I_{\mathrm{res1}}}{\pi V_1}}{3} \\ I_{\mathrm{res1}} = V_1 \sqrt{\dfrac{2C_{\mathrm{oss1}} Cr}{(2C_{\mathrm{oss1}} + Cr)Lr}} \\ |Z|_{\max} = \dfrac{M_G V_1^2 (6\phi_{\max} - \pi)}{6P_{\mathrm{tr},3\phi,\max}}. \end{cases} \tag{22}$$

The value of the resonant inductor and capacitor can be chosen as

$$\begin{cases} L_r = 20\ \mu\text{H} \\ C_r = 130\ \text{nF}. \end{cases}$$

The resonant current I_{res1} and I_{res2} can be determined by (13) and (16)

$$\begin{cases} I_{\text{res1}} = V_1\sqrt{\dfrac{2C_{\text{oss1}}Cr}{(2C_{\text{oss1}}+Cr)Lr}} = 1.44\ \text{A} \\ I_{\text{res2}} = V_2\sqrt{\dfrac{2C_{\text{oss2}}Cr}{(2C_{\text{oss2}}+n^2Cr)Lr}} = 0.16\ \text{A}. \end{cases}$$

Equation (19) indicates that the voltage ratio range is figured out

$$0.502 \le M_G \le 0.562.$$

$M_G = 0.56$ is selected within this range, and the turn ratio n is computed using the following expression:

$$n = \frac{M_G V_1}{V_2} = 14/3.$$

From (20), the range of the impedance Z is defined as

$$\begin{cases} |Z|_{1,\max} \le \dfrac{\pi V_1(2-3M_G)}{27I_{\text{res1}}} = 10.34 \\ |Z|_{2,\max} \le \dfrac{n\pi V_1(2M_G-1)}{9I_{\text{res2}}} = 488.7. \end{cases}$$

Therefore, the maximum switching frequency can be calculated as

$$|Z|_{\max} = 2\pi f_{s,\max}L_r - \frac{1}{2\pi f_{s,\max}C_r} \le 10.34$$

$$\Rightarrow f_{s,\max} \le 148\ \text{kHz}.$$

The maximum switching frequency is matched to the design. Therefore, the ZVS of all MOSFETs can be achieved when the operating switching frequency is under the range

$$f_r(=100\ \text{kHz}) \le f_s \le f_{s,\max}(=148\ \text{kHz}).$$

The digital signal processor (DSP) TMS320F28035 of Texas Instrument is employed to control the system. The control law accelerator module of this DSP with the interrupt frequency equal to the switching frequency is defined for better performance. Fig. 13 shows the simulation waveform of three-phase dc–dc converter operating in the buck and boost mode at 100% load. The shape of the inductor current is matched with the analysis. Moreover, the primary voltage is six-step and the secondary voltage is three-step as the same as shown in Fig. 5. The experimental waveforms of the buck and boost mode from light-load to full-load condition of phase one at the nominal input voltage ($V_1 = 400$ Vdc) are shown in Fig. 14. At the light-load condition, the switching frequency is high with a small phase shift value due to (10). The inductor current at the turned-ON of MOSFET S_A is negative and lower than I_{res1} from light load to full load. The secondary current also satisfies the ZVS condition for the secondary MOSFETs on the basis of (15). The ZVS is achieved in all MOSFETs from light-to full-load condition.

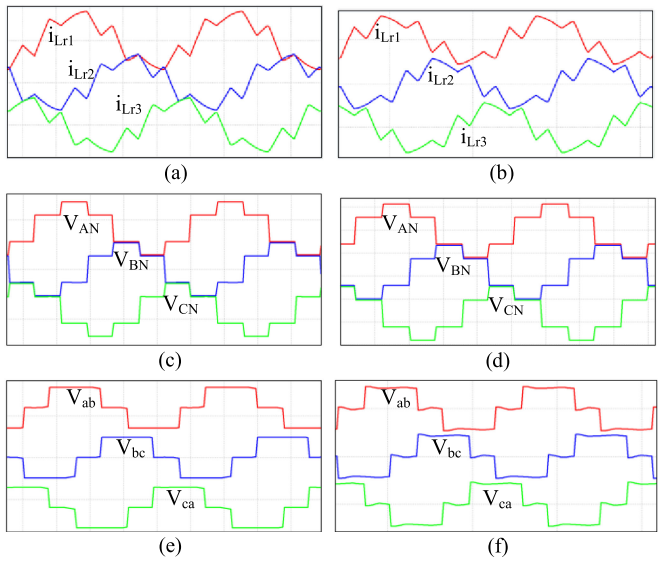

Fig. 13. Simulation waveform of the (a, c, e) buck and (b, d, f) boost modes at 100% load, respectively.

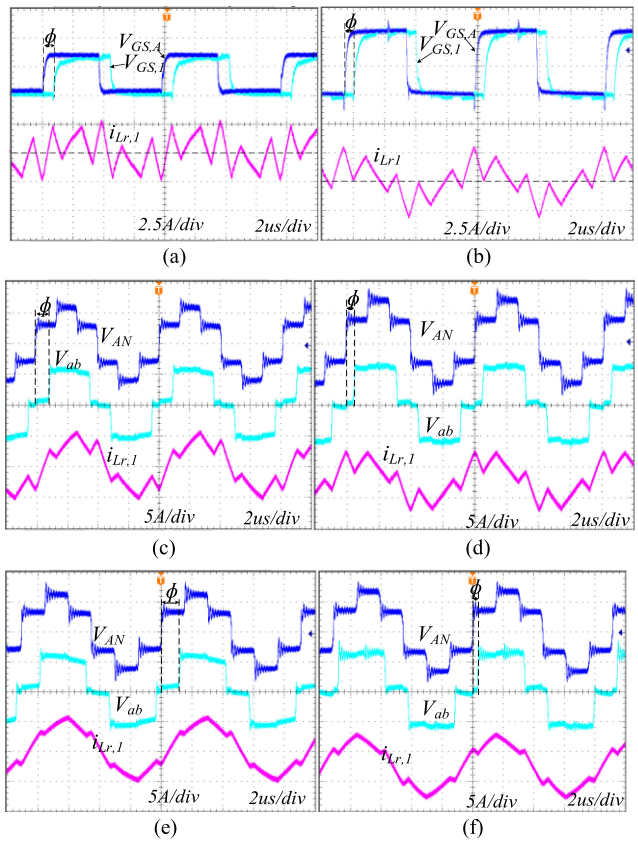

Fig. 14. Typical waveforms of the (a, c, e) buck mode and (b, d, f) boost mode at 10%, 50%, and 100% load.

Fig. 14(a), (c), and (e) illustrates that the frequency is reduced from 132 to 124.3 kHz and 111 kHz to regulate the output voltage and the phase shift is increased by (10) in the buck mode. In the boost mode, the frequency reduces from 131.3 to 124 kHz and 113.1 kHz, as shown in Fig. 14(b), (d), and (f). The primary transformer voltage is at two-thirds of input voltage, which is

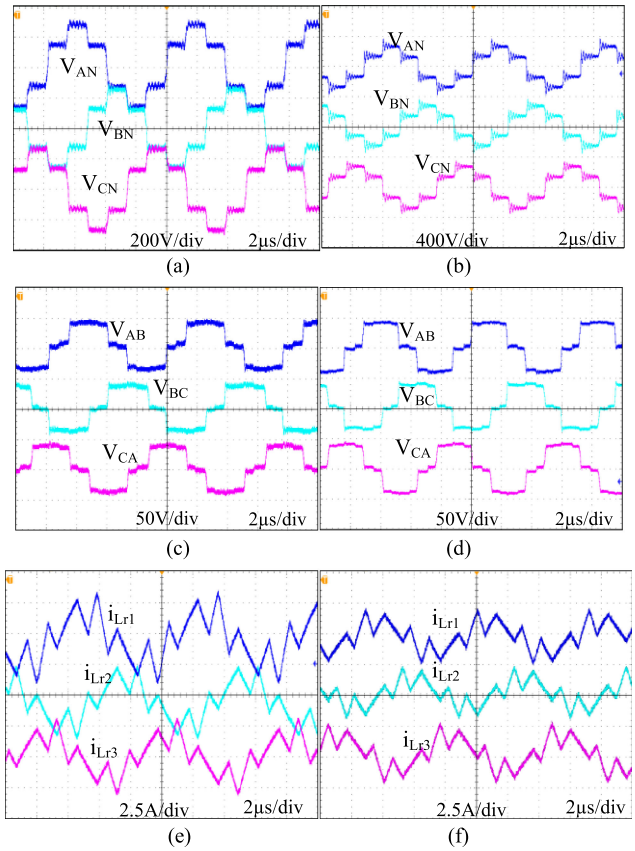

Fig. 15. Typical waveforms of (a, c, e) buck and (b, c, f) boost of the three-phase converter at 20% load.

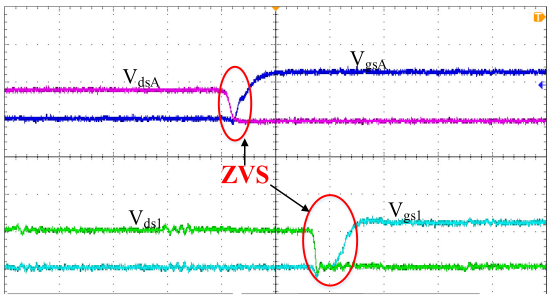

Fig. 16. ZVS of MOSFETs S_A and S_1 at 10% load in the buck mode.

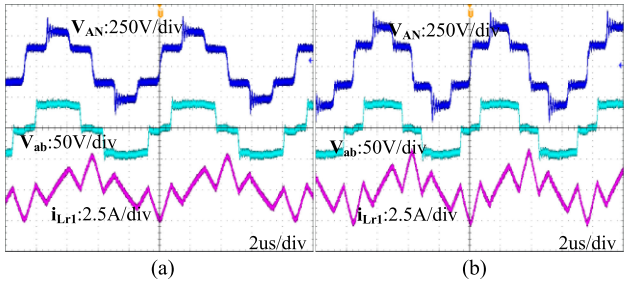

Fig. 17. Typical waveforms at 30% load. (a) 390 Vdc input voltage. (b) 420 Vdc input voltage.

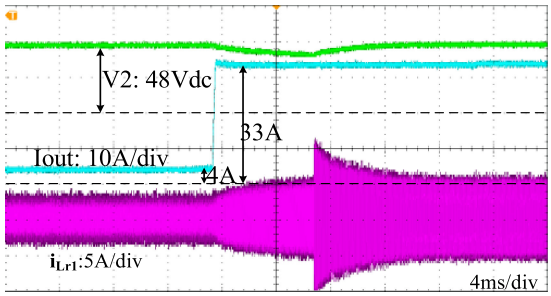

Fig. 18. Dynamic load from 10% to 80% load.

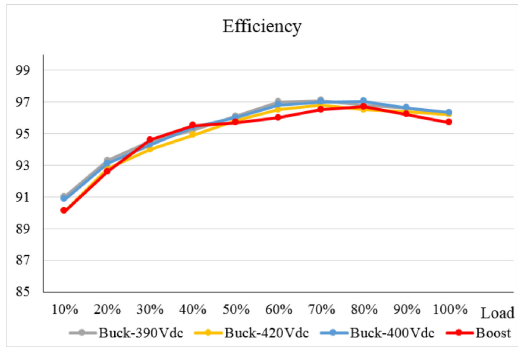

Fig. 19. Measured efficiency performance.

the advantage of the wye connection of the transformer. The small oscillation of the primary voltage V_{AN} is from the resonance formed by the resonant inductor and the output parasitic capacitor of the secondary MOSFETs. Moreover, because of the use of the free common node "*N*" in the wye connection of the transformers, it would cause the noise from the parasitic components of the transformers.

The primary and secondary voltage transformers and the inductor current of the three-phase converter waveforms at input voltage V_1 of 400 Vdc are shown in Fig. 15. Phases two and three exist phase shifts 120° and 240° with phase one, and the inductor currents of the three phases are balanced. In other words, the energy transfer of the three phases is balanced. Fig. 16 shows the ZVS of MOSFETs S_A and S_1 at 10% load in the buck mode. Whenever the inductor current fulfills the ZVS condition, the MOSFETs can achieve ZVS even at light-load condition. Fig. 17 shows the typical waveforms at 390 and 420 Vdc input voltage at 40% load. The inductor current and the transformer voltage keep the same with the analysis. To demonstrate the closed loop of the controller, the dynamic load from 10% to 80% is shown in Fig. 18. It is shown that the output voltage is well regulated. To limit the transient peak current, the time response of the controller was designed "slower." Fig. 19 shows the overall performance of the three-phase wye-delta converter in buck at minimum, maximum, and nominal input voltage and boost modes. The efficiency is quite high from light load to full load. The results show that a peak efficiency of 97.02% is achieved at the nominal input voltage. Fig. 20 shows the prototype of the three-phase wye-delta bidirectional converter.

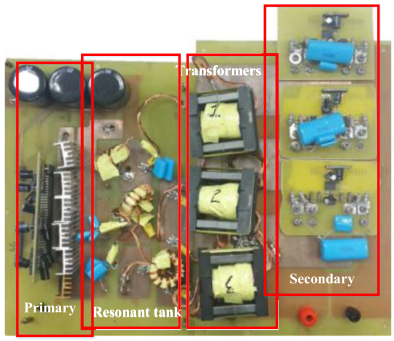

Fig. 20. Prototype of the bidirectional three-phase series resonant wye-delta converter.

V. Conclusion

A bidirectional three-phase wye-delta converter with a novel control modulation is proposed in this study. The wye-delta connection allows the stability of the battery side and reduces the voltage and current stress on the transformers. A novel control modulation with a frequency control and phase-shift control algorithm was employed to optimize the rms inductor current by limiting the small range of the switching frequency and to achieve the ZVS for all MOSFETs in the entire power range. A 2 kW prototype is built and successfully tested to verify this topology and the control modulation.

References

[1] P. F. Ribeiro, B. K. Johnson, M. L. Crow, A. Arsoy, and Y. Liu, "Energy storage systems for advanced power applications," *Proc. IEEE*, vol. 89, no. 12, pp. 1744–1756, Dec. 2001.

[2] J. Feng, Y. Hu, W. Chen, and C. C. Wen, "ZVS analysis of asymmetrical half-bridge converter," in *Proc. IEEE 32nd Annu. Power Electron. Spec. Conf.*, 2001, vol. 1, pp. 147–234.

[3] N. A. Dung, P. P. Hieu, Y. C. Hsieh, J. Y. Lin, Y. C. Liu, and H. J. Chiu, "A novel low-loss control strategy for bidirectional DC-DC converter," *Int. J. Circuit Theory Appl.*, vol. 45, pp. 1801–1813, Jun. 2017, doi: 10.1002/cta.2373.

[4] M. Ahmadi and K. Shenai, "New, efficient, low-stress buck/boost bidirectional DC- DC converter," in *Proc. IEEE Energy Tech*, pp. 1–6, 2012.

[5] F. C. Lee, "High-frequency quasi-resonant and multi-resonant converter technologies," in *Proc. IEEE 14th Annu. Conf. Ind. Electron. Soc.*, 1988, pp. 509–521.

[6] P. Thumalla, Z. Zhang, and M. A. E. Andersen, "High voltage bidirectional flyback converter for capacitive actuator," in *Proc. 15th Eur. Conf. Power Electron. Appl.*, 2013, pp. 1–10.

[7] M. Kim, M. Rosekeit, S. K. Sul, and R. W. De Doncker, "A dual phase-shift control strategy for dual active bridge DC-DC converter in wide voltage range," in *Proc. IEEE 8th Int. Conf. Power Electron. ECCE Asia*, 2011, pp. 364–371.

[8] M. Jafari, Z. Malekjamshidi, and J. G. Zhu, "Analysis of operation modes and limitations of dual active bridge phase-shift converter," in *Proc. IEEE 1th Int. Conf. Power Electron. Drive*, 2015, pp. 393–398.

[9] G. G. Oggier, R. Leidhold, G. O. Garcia, A. R. Oliva, J. C. Balda, and F. Barlow, "Extending the ZVS operating range of dual active bridge high-power DC-DC converters," in *Proc. IEEE 37th Power Electron. Spec. Conf.*, 2006, pp. 1–7.

[10] H. Kakigano, "Fundamental study on control strategies to increase efficiency of dual active bridge DC-DC converter," in *Proc. 41st Annu. Conf. IEEE Ind. Electron. Soc.*, 2015, pp. 1073–1078.

[11] B. Zhao, Q. Song, W. H. Liu, and Y. Sun, "Overview of dual active bridge isolated bidirectional DC-DC converter for high frequency link power conversion system," *IEEE Trans. Power Electron.*, vol. 29, no. 8, pp. 4091–4106, Aug. 2014.

[12] F. Krismer and J. W. Kolar, "Efficiency-optimized high-current dual active bridge converter for automotive applications," *IEEE Trans. Power Electron.*, vol. 59, no. 7, pp. 2745–2760, Jul. 2012.

[13] H. Wen and W. Xiao, "Bidirectional dual active bridge DC-DC converter with triple-phase-shift control," in *Proc. 28th Annu. IEEE Appl. Power Electron. Conf. Expo.*, 2013, pp. 1972–1978.

[14] Y. K. Lo and J. Y. Lin, "Active-clamping ZVS flyback converter employing two transformers," *IEEE Trans. Power Electron.*, vol. 22, no. 6, pp. 2416–2423, Nov. 2007.

[15] D. D. Nguyen, D. T. Nguyen, and G. Fujita, "Dual active bridge series resonant converter: A new control strategy using phase-shifting combined frequency modulation," *IEEE Trans. Power Electron.*, pp. 1215–1222, Sep. 2015.

[16] Z. Wang and H. Li, "Three-phase bidirectional dc-dc converter with enhanced current sharing capability," in *Proc. IEEE Energy Convers. Congr. Expo.*, 2010, pp. 1116–1122.

[17] H. M. O. Filho, D. S. Oliveira, Jr., and P. P. Praca, "Steady-state analysis of a ZVS bidirectional isolated three-phase DC-DC converter using dual-phase-shift control with variable duty cycle," *IEEE Trans. Power Electron.*, vol. 31, no. 3, pp. 1863–1872, Mar. 2016.

[18] Z. Wang and H. Li, "A soft switching three-phase current-fed bidirectional DC-DC converter with high efficiency over a wide input voltage range," *IEEE Trans. Power Electron.*, vol. 27, no. 2, pp. 669–684, Feb. 2012.

[19] A. Mohammadpour, T. Li, and L. Parsa, "Three-phase current-fed zero current switching phase-shift PWM DC-DC converter," *IEEE Trans. Power Electron.*, pp. 5079–5084, Sep. 2014.

[20] R. W. De Doncker, D. M. Divan, and M. H. Kheraluwala, "A three-phase soft-switched high power density DC-DC converter for high power applications," *IEEE Trans. Power Electron.*, vol. 27, no. 1, pp. 63–73, Jan./Feb. 1991.

[21] D. V. Ghodke, K. Chatterjee, and B. G. Fernandes, "Three-phase three-level, soft switched, phase shifted PWM DC-DC converter for high power applications," *IEEE Trans. Power Electron.*, vol. 23, no. 3, pp. 1214–1227, May 2008.

[22] H. Hoek, M. Neubert, and R. W. De Doncker, "Enhanced modulation strategy for a three-phase dual active bridge boosting efficiency of an electric vehicle converter," *IEEE Trans. Power Electron.*, vol. 28, no. 12, pp. 5499–5507, Dec. 2013.

[23] H. M. O. Filho, D. S. Oliveira, Jr., and C. E. Silva, "ZVS bidirectional isolated three-phase dc-dc converter with dual phase-shift and variable duty cycle," in *Proc. 10th IEEE/IAS Int. Conf. Ind. Appl.*, 2012, pp. 1–8.

[24] J. Huang, Y. Wang, Z. Li, Y. Jiang, and W. Lei, "Simultaneous PWM control to operate the three-phase dual active bridge converter under soft switching in the whole load range," in *Proc. IEEE Appl. Power Electron. Conf. Expo.*, 2015, pp. 2885–2891.

[25] R. Mirzahosseini and F. Tahami, "A phase-shift three-phase bidirectional series resonant DC-DC converter," in *Proc. 37th Annu. Conf. IEEE Ind. Electron. Soc.*, 2011, pp. 1137–1143.

[26] M. Rakesh, P. S. Satya, and A. Pramond, "Design and implementation of three-phase resonant DC-DC converter for low-voltage high-current applications," *J. Elect. Power Compon. Syst.*, vol. 42, pp. 1249–1265, 2014.

[27] F. X. Liu, Y. Chen, and X. L. Chen, "Comprehensive analysis of three-phase three-level LC-type resonant DC/DC converter with variable frequency control- series resonant converter," *IEEE Trans. Power Electron.*, vol. 32, no. 7, pp. 5122–5131, Jul. 2017.

[28] M. B. E. Kattel, R. Mayer, and S. V. G. Oliveira, "A three phase flyback current-fed push-pull bidirectional DC-DC converter for DC microgrid application," in *Proc. 12th IEEE Int. Conf. Ind. Appl.*, Mar. 2016, pp. 1–6.

[29] Y. K. Lo, J. Y. Lin, and C. Y. Lin, "Analysis and design of a half-bridge LLC series resonant converter employing two transformers," *Int. J. Circuit Theory Appl.*, vol. 40, pp. 985–998, 2011.

Nguyen Anh Dung (SM'14) was born in Binh Thuan province, Vietnam, in 1990. He received the B.S. degree from Ho Chi Minh City University of Technology, Ho Chi Minh City, Vietnam, in 2013, and the M.S. degree in 2015 from the National Taiwan University of Science and Technology, Taipei, Taiwan, where he is currently working toward the Ph.D. degree. His Ph.D. degree focuses on the digital control of power converter, bidirectional dc–dc converter for energy storage systems, and novel modulation of the dc–dc converter.

Huang-Jen Chiu (M'00–SM'09) has been with the Department of Electronic and Computer Engineering, National Taiwan University of Science and Technology, Taipei, Taiwan, where he is a Distinguished Professor and the Director of Center for Power Electronic Technologies. He also serves as a Vice Dean with the College of Electrical Engineering and Computer Science and a Vice Dean with the Office of Industry-Academia Collaboration.

Prof. Chiu was the recipient of several distinctive awards including the Young Researcher Award in 2004 from the Ministry of Science and Technology, Taiwan; the Outstanding Teaching Awards in 2009 and 2017 and the Excellent Research Award in 2009 and 2011 from the NTUST; the Y. Z. Hsu Scientific Paper Award in 2010; the Excellent Academic-Industry Collaboration Award in 2015 and 2017; and the Google Little Box Academic Awards. His student teams were the recipient of the grand prize of the IEEE International Future Energy Challenge (IFEC) in 2013 and 2015, respectively. He serves as an Associate Editor of the IEEE TRANSACTIONS ON INDUSTRY APPLICATIONS and an Associate Editor of the IEEE TRANSACTIONS ON CIRCUITS AND SYSTEMS PART II: EXPRESS LETTERS (TCAS-II). He is actively working in IEEE Taipei Section. He arranged several meetings to promote the local activity of IEEE member in Taipei Section and to increase the number of IEEE membership in Taiwan. He served as the Chair of IEEE Industrial Electronics Society Taipei Chapter (2015–2016), the General Co-Chair of the 2017 IEEE International Future Energy Electronics Conference (IFEEC 2017-ECCE Asia), the Program Chair of the 2015 IEEE International Future Energy Electronics Conference (IEEE IFEEC 2015), the Topic Co-Chair of the IFEC 2016, and the Secretary of IEEE PELS/IES Taipei Joint Chapter during 2010–2014. He is a Fellow of the Institute of Engineering and Technology and selected as the Distinguished Lecturer of the IEEE Power Electronics Society (2017–2018).

Jing-Yuan Lin (M'14) was born in Kao-Hsiung, Taiwan, R.O.C. He received the M.S. and Ph.D. degrees in electronic engineering from the National Taiwan University of Science and Technology, Taipei, Taiwan, in 2002 and 2007, respectively.

In 2013, he was with the faculty of the Department of Electrical Engineering, National Taitung Junior College, Taitung, Taiwan. Since 2014, he has been with the faculty of the Department of Electronic, National Taiwan University of Science and Technology, where he is currently an Assistant Professor. His research interests include the design and analysis of zero-voltage-switching dc–dc converter, power factor correction techniques, converter modeling, and power IC design.

Yao-Ching Hsieh (M'04) was born in Kaohsiung, Taiwan, in 1969. He received the B.E. and M.S. degrees from National Taiwan University, Taipei, Taiwan, in 1991 and 1993, respectively, and the Ph.D. degree from National Sun Yat-sen University, Kaohsiung, Taiwan, in 2004, all in electrical engineering.

From August 1996 to July 2006, he was a Lecturer with the Kao-Yuan Institute of Technology, Kaohsiung. Initially with the Department of Information System and then he transferred to be with the Department of Electrical Engineering. Beginning from August 2006, he was with the Department of Electrical Engineering, National Dong Hwa University, Hualien, Taiwan, where he was first an Assistant Professor and then became an Associate Professor in 2009. During 2014 and 2017, he was with the Department of Electronic and Computer Engineering, National Taiwan University of Science and Technology, Taipei. Since September 2017, he has been with the Department of Electrical Engineering, National Sun Yat-sen University. His research interests include battery-related technology, soft switching techniques, and power converters.

Hui-Ting Chen was born in Taipei, Taiwan, in 1991. He received the M.E. degree from the National Taiwan University of Science and Technology, Taipei City, Taiwan, in 2017.

His research interests include high efficiency/high power density dc–dc converters and power factor correction (PFC) topologies.

Bo-Xiang Zeng was born in Nantou, Taiwan, in 1994. He received the B.E. degree from the Oriental Institute of Technology, New Taipei, Taiwan, in 2016. He is currently working toward the M.E. degree at the National Taiwan University of Science and Technology, Taipei, Taiwan.

His research interests include high efficiency/high power density bidirectional dc–dc converters, PFC topologies, and DSP control application.